

Generalized Moment Cancellation for Long-Range Electrostatics

B. Stenqvist,^{1, a)} Vidar Aspelin,² and Mikael Lund^{2, b)}¹⁾*Department of Chemistry, Division of Physical Chemistry, Lund University, Sweden*²⁾*Department of Chemistry, Division of Theoretical Chemistry, Lund University, Sweden*

(Dated: 24 April 2019)

Evaluating long-range electrostatics using a short-range pair potential is appealing in that computational complexity scales linearly with the number of particles. Existing models – with or without arbitrary damping parameters – cancel electric multipole moments within a small cut-off sphere to account for the long-range medium response. We here present a rigorous and formally exact new method that cancels up to *inifinitely* many multipole moments and is free of damping parameters. Using molecular dynamics simulations of a point charge water model, we discuss radial distribution functions, Kirkwood-Buff integrals, dielectrics, and angular correlations in relation to existing electrostatic models. While cancelling 2 – 5 moments, we find that the proposed method is an efficient and accurate alternative for handling long-range electrostatics as compared to the standard Ewald summation.

PACS numbers: Valid PACS appear here

Keywords: Electrostatics, Pair-potential, Poisson equation, Yukawa potential, SPC/E-water, Gaussian charge-distribution

I. INTRODUCTION

Accurate and efficient algorithms to calculate long-ranged electrostatic interactions is important to expand time and space in atomistic simulations. One of the earliest such methods is the reaction field method¹ where a spherical cut-off, R_c , is applied. Outside of this cut-off the potential is zero, and hence the computational effort is roughly $\mathcal{O}(\mathcal{N})$, where \mathcal{N} is the number of particles in the system. However, to correctly parametrize the reaction field the dielectric constant, ε_r , needs to be evaluated. Ewald methods^{2,3} provide an accurate electrostatic description within a well known parameter-space^{4,5} for a *periodic* system. The computational time is roughly $\mathcal{O}(\mathcal{N}^2)$, however, with optimal parameters it scales as $\mathcal{O}(\mathcal{N}^{3/2})$. This exponential cost with increasing system size makes it demanding for large systems, albeit derived versions such as Particle Mesh Ewald⁶ (PME) under such conditions scales as $\mathcal{O}(\mathcal{N} \log(\mathcal{N}))$. Alternative methods with both high efficiency and accuracy such as the charge neutralizing Wolf method⁷ has been thoroughly tested and validated, and evolved^{8–11} in order to further reduce this still high computational cost. Evolutions from the original Wolf formalism are primarily based on cancellation of the derivative of the potential at the cut-off, convenient since Molecular Dynamics simulations require just this. Such cancellation of the derivative may be equivalent to cancel an introduced dipolar artefact¹². By expanding from the Wolf method, we here show that cancelling *every* electrostatic moment is equivalent to taking all long-ranged interactions into account. We present a potential which in addition to cancel arbitrarily (including infinitely) many moments, cancels equally many

higher derivatives at the cut-off. From a physical viewpoint this is reasonable as to avoid truncation errors; a conjecture that has previously been brought forward⁹. A similar approach of higher order moment-cancellation has recently been presented¹³, nevertheless, an arbitrary damping-parameter was introduced in addition to the cut-off parameter. The approach presented in this work requires a cut-off and choosing how many moments, P , to cancel. P thus connects directly to physical properties of the examined system, and the arbitrary damping-parameter in other similar formalisms is avoided. Furthermore, the presented theory may also be applicable in other systems which relies on moment cancellation, such as for example noise reduction in automatic control systems.

II. THEORY

The electrostatic pair-interaction energy u_{ij} between charges z_i and z_j inside a spherical cut-off can for all here examined models be written as a function of separation r ,

$$u_{ij} = \frac{e^2 z_i z_j}{4\pi\varepsilon_0\varepsilon_r r} \mathcal{S}(q) \quad (1)$$

where the splitting function, $\mathcal{S}(q)$, is defined in Table I using $q = r/R_c$ and $\mathcal{S}(q) \equiv 0$ for $q > 1$. In Eq. 1, e is the elementary charge, ε_0 is the vacuum permittivity, and ε_r the relative permittivity. The new method presented here, which we denote the “ q -potential”, cancel an arbitrary number of electrostatic moments and derivatives P at the cut-off, and is defined by the splitting function,

$$\mathcal{S}(q) = \prod_{n=1}^P (1 - q^n). \quad (2)$$

In the next section we will show how it is derived.

^{a)}Electronic mail: bjorn.stenqvist@teokem.lu.se

^{b)}Electronic mail: mikael.lund@teokem.lu.se

label	$\mathcal{S}(q)$	ref.
q -potential	$\prod_{n=1}^P (1 - q^n)$	this work
Ewald, real-space	$\text{erfc}(q\kappa)$	2
SP1	$(1 - q)^2$	10
SP3	$(1 + 2.25q + 3q^2 + 2.5q^3)(1 - q)^4$	11

TABLE I: Splitting functions, $\mathcal{S}(q)$ for various electrostatic schemes. To simplify we have used $\kappa = \alpha R_c$ where α is the commonly used damping-parameter. We want the reader to note that SP stands for 'shifted potential' and the number suffix stands for how many derivatives that are zero at the cut-off.

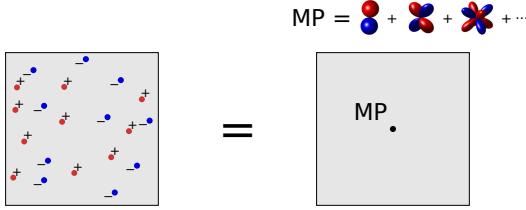


FIG. 1: Conversion of a cell with point-charge particles (left) to a cell with a single centered point-multipole particle MP (right).

A. Generalized Moment Cancellation

The total interaction energy between \mathcal{N} charged particles using periodic boundary conditions is

$$E_{\text{Tot}} = \frac{e^2}{4\pi\epsilon_0\epsilon_r} \frac{1}{2} \sum_{\mathbf{n} \in \mathbb{Z}^3} \sum_{i=1}^{\mathcal{N}} \sum_{j=1}^{\mathcal{N}} z_i \mathbf{T}_0(\mathbf{r}_{ij} + \mathbf{n} \circ \mathbf{L}) z_j. \quad (3)$$

Here the prime indicates that $i \neq j$ when $\mathbf{n} = \mathbf{0}$, \circ denotes the Hadamard product, and \mathbf{r}_{ij} is the distance-vector between the point-charges i and j . The size of the cuboid cell is described by its side-lengths, $\mathbf{L} = (L_x, L_y, L_z)$. The zeroth order interaction-tensor $\mathbf{T}_0(\mathbf{r})$ is here introduced as

$$\mathbf{T}_0(\mathbf{r}) = \frac{1}{|\mathbf{r}|}. \quad (4)$$

By assuming $\sqrt{L_x^2 + L_y^2 + L_z^2}/2 < \min(L_x, L_y, L_z)$, it is possible to convert all point-charge particles in each replicated cell into a single centered point-multipole particle represented by infinitely many higher order moments, see Fig. 1. This conversion to a point-multipole particle is valid since the center of any reciprocal point-multipole particle $(n_x L_x, n_y L_y, n_z L_z)$ is located further away from the origin of the centered cell ($\min(|n_x L_x, n_y L_y, n_z L_z|) = \min(L_x, L_y, L_z)$) than any point-charge particle in the centered cell itself, $\max(|\mathbf{r}_{ij}|) = \sqrt{L_x^2 + L_y^2 + L_z^2}/2$. If every moment of every such point-multipole particle is a zero-tensor, then there would not be any interactions between reciprocal cells. For such a system the interaction-energy would simply be

$$E_{\text{Tot}} = \frac{e^2}{4\pi\epsilon_0\epsilon_r} \frac{1}{2} \sum_{i=1}^{\mathcal{N}} \sum_{j=1}^{\mathcal{N}} z_i \mathbf{T}_0(\mathbf{r}_{ij}) z_j. \quad (5)$$

Hence, if we construct an effective potential which cancels the total electrostatic moments of the cell, then the total interaction energy would be given solely from the particles in the centered box. This can be regarded as a reaction field approach where the induced field exactly cancels every moment locally. For higher order interactions than dipole-dipole and ion-quadrupole interactions, the long-ranged interactions is absolutely convergent. Thus the highest order moment that needs to be cancelled is the quadrupole moment.

Our conjecture is that an electrostatic potential based on moment cancellation can be described by the potential from the original particle and P image particles. We denote the aggregated potential from the original and all image particles as V_q , which is a function of the distance-vector \mathbf{r} and the charge z ,

$$V_q(\mathbf{r}, z) = V(\mathbf{r}, z) + \sum_{p=1}^P V(\mathbf{r}_p, z_p). \quad (6)$$

Here V symbolized the Coulomb potential, z the charge of the original particle, z_p the charge of image particle p , and $\mathbf{r}_p = c_p \mathbf{r}$ where c_p is a proportionality factor to be discussed. The requirement that all, up to M , higher order moments of all image particles should cancel the original particle moments, can be formulated in a single tensor-equation as

$$\begin{bmatrix} 1 \\ r \\ \vdots \\ r^M \end{bmatrix} z + \begin{bmatrix} 1 & 1 & \dots & 1 \\ r_1 & r_2 & \dots & r_P \\ \vdots & \vdots & \ddots & \vdots \\ r_1^M & r_2^M & \dots & r_P^M \end{bmatrix} \begin{bmatrix} z_1 \\ z_2 \\ \vdots \\ z_P \end{bmatrix} = \begin{bmatrix} 0 \\ 0 \\ \vdots \\ 0 \end{bmatrix}. \quad (7)$$

Here r is any component of \mathbf{r} , and r_p is any component of \mathbf{r}_p . The meaning of line m in Eq. 7 is that the $m-1$ order moment from the original particle (first term; $r^{m-1}z$) together with the sum of the same order moments of the image particles (second term; $\sum_{p=1}^P r_p^{m-1}z_p$) should equal zero (right-hand-side). If we assume the image particle positions r_p to be unique, and the matrix to be square (*i.e.* $M = P - 1$), we ensure a solution exists. Then, by choosing the positions r_p we can extract the charges z_p . The positions of the image particles may be arbitrary chosen, with exceptions mentioned earlier, however in this work we use $c_p = q^{-p}$. That is, the position of image particle $p+1$ (r_{p+1}) is the mirror image of the position of image particle $p-1$ (r_{p-1}) in the position of image particle p (r_p), *i.e.* $r_p^2 = q^{-2p}r^2 = q^{-(p-1)}r q^{-(p+1)}r = r_{p-1}r_{p+1}$. Using these assumptions together with Eq. 7 yields the solution for the image charges as (for details see Appendix A)

$$z_p = z \cdot \begin{bmatrix} P \\ p \end{bmatrix}_q (-1)^p q^{p(p-1)/2}, \quad (8)$$

which is independent of r . Here $\begin{bmatrix} P \\ p \end{bmatrix}_q$ is the q -analogue of the binomial coefficients¹⁴. With the use of Eq. 8 it is

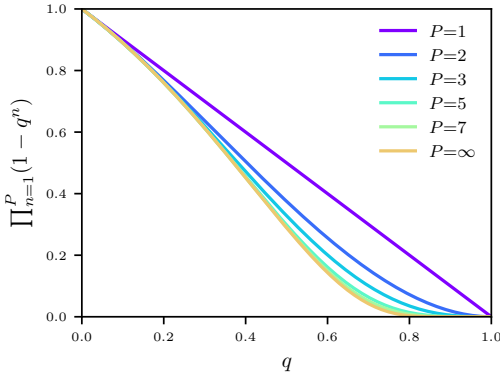


FIG. 2: The splitting-function $\mathcal{S}(q) = \prod_{n=1}^P (1 - q^n)$ for different numbers of cancelled moments.

possible to present an expression for the aggregated potential V_q . The modified ionic interaction-tensor is then

$$\mathbf{T}_0^q(\mathbf{r}) = \mathbf{T}_0(\mathbf{r}) \left(1 + \sum_{p=1}^P \frac{[P]_q (-1)^p q^{p(p-1)/2}}{q^{-p}} \right). \quad (9)$$

Here the expression within the parenthesis is composed of the contributions from the original particle (the 1) and all image particles (the sum). Rearranging and simplifying¹⁵ this expression gives

$$\mathbf{T}_0^q(\mathbf{r}) = \mathbf{T}_0(\mathbf{r}) \prod_{n=1}^P (1 - q^n) = \mathbf{T}_0(\mathbf{r})(q; q)_P \quad (10)$$

where $(a; q)_P$ is the q -Pochhammer Symbol. In Fig. 2 we show this multiplicative modification to the original interaction-tensor for different P . Finally, since the multiplicative term is a q -analogue of the Pochhammer symbol we address the proposed potential as the q -potential.

B. Self energy

A pair-interaction entails two particles and we have so far cancelled the moments of one of them, more specifically the one at distance r from the origin, assuming the other one is located in the origin. Thus the charge of the origin-located particle has not been cancelled, which we will now do. We have defined the resulting energy from this procedure as the *self energy*. The approach is in line with the previous derivation for the q -potential however for a detailed derivation see Appendix B which culminates into

$$E_{\text{Self}} = -\frac{e^2}{4\pi\epsilon_0\epsilon_r R_c} \sum_{i=1}^{\mathcal{N}} z_i^2 \quad (11)$$

C. Cancelled derivatives

In the following we show that the number of cancelled derivatives at the cut-off equals the number of cancelled

higher order moments. Using the general Leibniz rule, the N th derivative of the modified interaction-tensor becomes

$$\mathbf{T}_0^q(\mathbf{r})^{(N)} = \sum_{n=0}^N \binom{N}{n} (q; q)_P^{(n)} \mathbf{T}_0(\mathbf{r})^{(N-n)} \quad (12)$$

where the parenthesized index indicates the order of the derivative with respect to r . $\mathbf{T}_0(\mathbf{r})^{(N-n)}$ is non-zero for finite r and thus we focus on the $(q; q)_P^{(n)}$ -terms. The first derivative of $(q; q)_P$ is

$$(q; q)_P^{(1)} = \sum_{i=1}^P \frac{-iq^{i-1}}{R_c} \cdot \frac{(q; q)_P}{(1 - q^i)}. \quad (13)$$

Since the first factor of the term in the sum, $-iq^{i-1}/R_c$, is negative for all $i, q \in (0, 1]$, and $R_c > 0$, we conclude that $(q; q)_P^{(1)} = 0$ if and only if $(q; q)_P/(1 - q^i) = 0$ for any $i \in [1, P]$. For $i \in [1, P - 1]$ this is always true since after cancellation with the corresponding $(1 - q^i)$ term in $(q; q)_P$ the factor $(1 - q^P)$ is always left, which gives $\lim_{q \rightarrow 1^-} (q; q)_P/(1 - q^i) = 0$. Thus we move on and focus on the term $(q; q)_P/(1 - q^P)$ which can also be written as $(q; q)_{P-1}$. We now have a relationship between $(q; q)_P^{(1)}$ and $(q; q)_{P-1}$, if one is zero then so is the other. Since $\lim_{q \rightarrow 1^-} (q; q)_{P-1}$ is zero only when $P - 1 > 0$, the first derivative is zero at the cut-off only if $P > 1$. By repeating these arguments we get a relationship between $(q; q)_P^{(n)}$ and $(q; q)_{P-n}$. Like above, $\lim_{q \rightarrow 1^-} (q; q)_{P-n} = 0$ only when $P - n > 0$ and thus the maximal derivative to be zero at the cut-off is $n = P - 1$. Hence the number of cancelled *higher* order moments, $P - 1$, equals the number of *higher* order derivatives that is zero at the cut-off.

Furthermore, we note that by using the splitting-function $(q^d; q^d)_P$ where $d \in [1, 2, 3, \dots)$, $d - 1$ higher order derivatives are cancelled at $q = 0$. This is straightforward to acknowledge since the lowest power of q in $(q^d; q^d)_P$ (save $q^0 = 1$) is q^d . That is, the d th derivative of $(q^d; q^d)_P$ is the lowest order derivative (save zero) which does not vanish at $q = 0$, and therefore the $(d - 1)$ th derivative is the highest order derivative to vanish at $q = 0$ (given that $P > 0$). Thus we can independently tune how many derivatives to cancel at $q = 0$ (using d) and at $q = 1$ (using P). In this work we have made the restriction $d = 1$.

D. Potential for systems with moments

While the no net moment assumption is fair for many liquids, it generally does not describe systems with dipolar or ferroelectric properties. Therefore we now suggest a generalization of the method for such cases. Earlier we noted that to cancel every moment within a cut-off region gives the right-hand side of Eq. 7 as the zero-vector. If however there should be a non-zero moment within this region, one gets Eq. 14 where $\Psi^{(p)}$ is the p th higher order moment in the region projected onto the r -component of \mathbf{r} . The solution to this equation is obviously more comprehensive than the solution to Eq. 7, yet it is solvable

(at least given the restrictions on r_p and M mentioned in Sec. II A) and hence we highlight the possibility to expand the q -potential for non-zero moment environments.

$$\begin{bmatrix} 1 \\ r \\ \vdots \\ r^M \end{bmatrix} z + \begin{bmatrix} 1 & 1 & \dots & 1 \\ r_1 & r_2 & \dots & r_P \\ \vdots & \vdots & \ddots & \vdots \\ r_1^M & r_2^M & \dots & r_P^M \end{bmatrix} \begin{bmatrix} z_1 \\ z_2 \\ \vdots \\ z_P \end{bmatrix} = \begin{bmatrix} \Psi^{(0)} \\ \Psi^{(1)} \\ \vdots \\ \Psi^{(M)} \end{bmatrix}. \quad (14)$$

E. Choosing the cut-off

It is desirable to use a minimal cut-off to speed up calculation time. The physical interpretation of such a cut-off, which still accurately describes the system, is the smallest region exhibiting manageable deviations within the no net moment approximation, correctable by induced conductive image particles. It is formally sound to use a larger cut-off since every larger region should also display the same quality. Yet, most systems does display a certain local anisotropy, or equivalently, non-vanishing moments. The cut-off thus needs to be large enough to at least enclose this space, however to ensure no inter-cell correlations between anisotropic regions, it should not exceed a fourth of the shortest cell-length¹⁶, which for a spherical cut-off is $\min(L_x, L_y, L_z)/4$. Note that the no net moment approach does not require an isotropic cut-off but can rather take the shape of any closed space.

III. METHODS

A. Molecular Dynamics Simulation

All simulations were performed in the isobaric-isothermal (\mathcal{NPT}) ensemble at pressure $\mathcal{P} = 1$ bar and temperature $T = 298.15$ K, using OpenMM 7.0.1¹⁷. The pressure was kept constant using a Monte Carlo barostat¹⁸ and we used a Langevin integrator¹⁹, with a friction coefficient of 1.0 ps and a time step of 2.0 ps, to keep constant temperature. Before production runs, the systems were energy minimized, then equilibrated. For simulations of only SPC/E water molecules, $\mathcal{N} = 2000$ and the production runs spanned 10 ns. The reference Ewald simulations utilized a fractional force error tolerance of $5 \cdot 10^{-4}$. Three different (real-space) cut-off distances were tested for all electrostatic schemes: 0.96 nm, 1.28 nm, and 1.60 nm. While we only present results using $R_c = 1.28$ nm in Sec. IV, the others are presented in Appendix C. Systems containing SPC/E water molecules and NaCl/NaI ions were simulated in order to retrieve activity derivatives according to Kirkwood-Buff theory as is described in the next section. The simulations were carried out in a cubic box of volume $\sim 6^3$ nm³ with $\mathcal{N} = 4402 - 5963$ water molecules depending on the type and concentration of electrolyte according to the values presented in Table VI in Appendix D. The production runs spanned 40 ns where we used PME as the reference

for the summation of the long-range electrostatic interactions. The fractional force error tolerance was the same as in the Ewald simulations.

B. Kirkwood-Buff Theory

The Kirkwood-Buff (KB) theory provides a general way to obtain macroscopic properties of a solution from its microscopic properties²⁰. The central property is the Kirkwood-Buff integral (KBI) between components A and B , defined as

$$G_{AB} = 4\pi \int_0^\infty [g_{AB}^{\mu VT}(r) - 1] r^2 dr \quad (15)$$

where $g_{AB}^{\mu VT}(r)$ is the radial distribution function (RDF) in the grand canonical ensemble (*i.e.* an open system), and r is the distance between the components. To obtain approximate KBIs in a closed system, the integral is typically truncated at a distance R after which the RDFs converge, and the grand-canonical RDF is replaced by the RDF computed in the closed system^{21,22}. However, to obtain accurate approximate KBIs according to this procedure, corrections are needed to compensate for the introduced errors. We here followed a procedure²³ in which two corrections^{24,25} are applied simultaneously to the KBIs. These correction factors are further explained in Appendix D. The derivative of the electrolyte activity at constant pressure, and temperature, is obtained according to²⁶

$$a'_c = \left(\frac{\partial \ln a_c}{\partial \ln \rho_c} \right)_{\mathcal{P}T} = \frac{1}{1 + \rho_c(G_{cc} - G_{wc})} \quad (16)$$

where for G_{cc} and G_{wc} , we used the corresponding truncated, corrected KBIs obtained from simulations, $\hat{G}_{cc}^*(R)$ and $\hat{G}_{wc}^*(R)$ (see Appendix D). Here subscripts c and w denote electrolyte and water respectively, $a_c = \gamma_c \rho_c$ is the electrolyte activity, γ_c is the molar mean activity coefficient of the electrolyte, and ρ_c is the number density of the electrolyte. Experimental activity derivatives for the simulated electrolytes were calculated from previously reported activity coefficients²⁷, using the fitting procedure described in Appendix D. For the simulations, we used one force field²⁸ for the Na⁺ and I⁻ ions while another²⁹ was used for Cl⁻. The parameters of these force fields are presented in Table VI in Appendix D.

IV. RESULTS AND DISCUSSION

To evaluate the developed q -potential we now investigate a bulk water system as well as an aqueous salt solution by analyzing, among others, radial distributions functions, angular correlations, and Kirkwood-Buff integrals. While the Ewald/PME methods assume a replicated environment and may thus not necessarily represent a true isotropic system^{16,30}, we choose this as our reference system due to its widespread use in molecular simulations. Thus, all results are compared against Ewald/PME.

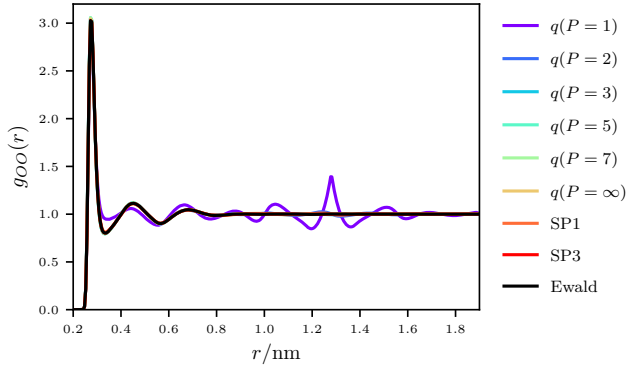


FIG. 3: Oxygen-oxygen pair-correlation function $g_{OO}(r)$. We want the reader to note that all but the $q(n=1)$ -curve overlap.

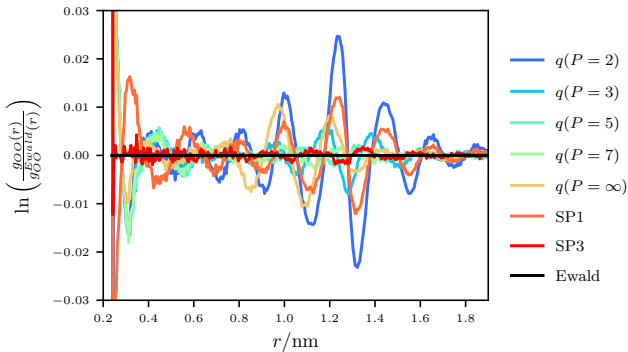


FIG. 4: The logarithm of the ratio between the pair-potential and Ewald results.

A. Bulk water-system

The radial distribution function between water oxygen atoms is presented in Fig. 3, and we see that the $q(P=1)$ -potential stands out with a peak at the cut-off distance 1.28 nm. The other potentials are harder to differentiate why we in Fig. 4 present the ratio between the pair-potential and Ewald results on a logarithmic scale. By initially increasing the order P from 2, we get results closer resembling Ewald. However, by using $q(P=\infty)$ we diverge from the Ewald-like results retrieved by the $q(P=5)$ - and $q(P=7)$ -potentials. There is thus a limit on how many cancellations are appropriate. The SP1-approach cancels one derivative at the cut-off and resembles Ewald more than by using the similar $q(P=2)$ -potential, yet more unlike results than if one uses $q(P=3)$. The SP3-approach, which cancels three derivatives at the cut-off, produces among the most Ewald-like results in this test akin the $q(P=5)$ and $q(P=7)$ results. Oddly, the SP3-potential is more comparable to q -potentials which cancel a fewer higher order derivatives than the same. Though the discrepancies between the pair-potentials and Ewald are oscillating, the peaks consistently occur around the cut-off distance. The difference between pair-potential and Ewald water-dipole correlations is presented in Fig. 5. The patterns are

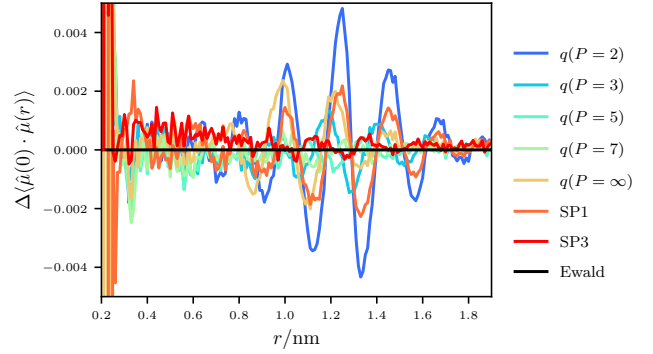


FIG. 5: Difference compared to Ewald results between angular correlations of the normalized dipole-moments $\hat{\mu}$ of the waters.

markably similar to the results in Fig. 4, thus leaving nothing new to add.

The density, dielectric constant (see Appendix E), and Kirkwood factor G_K , see Eq. 17, for the different potentials are presented in Table II. Again we note that $q(P=1)$ gives distinctly different results than the others. The densities for the other q -potentials are slightly below one. Contrary to the q -potential, both SP1 and SP3 give lower densities than Ewald and experimental values. The dielectric constant is irregular in P , yet for all $q(P > 1)$, SP1, and SP3 it is reasonable compared to primarily Ewald but also experimental results. Note however that $q(P=6)$ consistently gives a somewhat high dielectric constant compared to the others, independently of cut-off (see Appendix C). The Kirkwood factor indicates that the $q(P=1)$ -potential has large fluctuations of the dipole moment in the cell, which is paradoxical given the low dielectric constant. However, the derived formula for ϵ_r using the $q(P=1)$ -potential is known to represent high dielectric medium poorly³¹.

$$G_K = \left\langle \sum_{i=1}^{\mathcal{N}} \sum_{j=1}^{\mathcal{N}} \cos(\hat{\mu}_i \cdot \hat{\mu}_j) \right\rangle \quad (17)$$

In Appendix C we present bulk system results for different cut-offs, $R_c = 0.96$ nm and $R_c = 1.60$ nm, which gives slightly different RDFs than by using $R_c = 1.28$ nm. From Sec. II E however we note that the cut-off should obey $R_c < \min(L_x, L_y, L_z)/4$ and therefore, since the box-length is ~ 3.9 nm, artifacts may be present in systems using excessive cut-offs.

B. Salt solutions

Fig. 6 shows activity derivatives for NaCl and NaI solutions and the $q(P=3)$ -potential generally gives the most accurate results as compared to PME. For high molalities the potentials - including PME - starts to diverge from the experimental results. Note however that the $q(P=2)$ -potential most often resembles experimental results more closely than the others. By increasing the

Potential	ρ	ε_r	G_K
$q(P=1)$	1104	2 ± 0	2.8
$q(P=2)$	1000	70 ± 3	2.5
$q(P=3)$	999	71 ± 1	2.5
$q(P=4)$	999	68 ± 3	2.4
$q(P=5)$	999	67 ± 1	2.4
$q(P=6)$	999	76 ± 3	2.7
$q(P=7)$	999	71 ± 2	2.5
$q(P=8)$	998	71 ± 1	2.5
$q(P=\infty)$	999	72 ± 4	2.5
SP1	993	69 ± 3	2.4
SP3	995	71 ± 1	2.5
Ewald	996	66 ± 2	2.3
Exp.	997	79	-

TABLE II: Values for density ρ in units of kg/m^3 , dielectric constant ε_r , and Kirkwood factor G_K for the different potentials applied on a bulk water-system and experimental reference³².

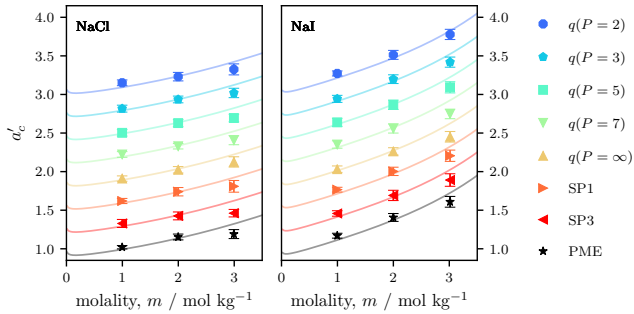


FIG. 6: Activity derivatives for NaCl (left) and NaI (right) using different potentials. The curves are shifted in steps of 0.3 from the PME results.

number of cancelled higher order moments/derivatives, the results increasingly differ from the experimental results. Here, low cancellation of moments gives the most accurate results. We have performed simulations using the $q(P=1)$ -potential with poor outcome (akin for the RDF), hence we again conclude that cancellation of a finite number, larger than one, is needed to capture the nature of the system. However, while evaluating KB integrals (still subjected to the previous restriction) a minimal number of cancelled moments/derivatives reproduce experimental results whereas increasing this number gives better agreement with PME. Still, we conclude by noting that all of the potentials give fair results for low/medium molalities.

The reasons for the pair-potentials to reproduce PME activity derivatives may either be that the RDFs are the same, or that the errors cancel while integrating to get the KBIs. Fig. 7 shows the RDFs between water and salt where we see that they do indeed differ from the PME results. The oscillating difference between pair-potential and PME RDFs does therefore not necessarily pose an obstacle in retrieving PME-like KBIs since the integrated errors cancel.

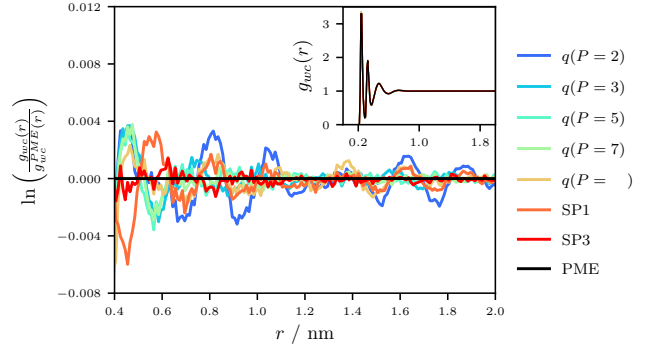


FIG. 7: The logarithm of the ratio between the water-ion RDFs from the pair-potential and from PME, for NaCl solutions with a salt concentration of 2.0 mol kg^{-1} . In the inset, the water-ion RDFs for all simulated potentials are shown.

V. CONCLUSION

We have presented a new theory for electrostatic interactions which relies on moment or derivative cancellation and has computational complexity of $\mathcal{O}(\mathcal{N})$. It can be regarded as a generalization of the Wolf method⁷ and has the advantages that it (i) allows for cancellation of *any* number of moments; (ii) is free of damping parameters otherwise needed for similar algorithms; (iii) is mathematically rigorous and has a simple form; (iv) reproduces results from Ewald/PME summation techniques for water and electrolyte solutions.

Results for solution structure, dielectric properties, and activity derivatives of aqueous, electrolyte systems agree with Ewald/PME for $P \in [2, 5]$ number of cancelled moments. The q -potential method is thus a valid alternative to Ewald/PME at a lower computational cost. Finally, we note that the methodology can be expanded to multipolar interactions and thus applicable also for explicit polarization simulations.

ACKNOWLEDGMENTS

We thank LUNARC for computational resources and for financial support: Södra Research foundation; the Swedish Research Council; and the Swedish Foundation for Strategic Research.

Appendix A: Derivation of image charges

By using $r_p = c_p r$ and $\hat{z}_p = z_p/z$ it is possible to transform Eq. 7 into Eq. A1.

$$\begin{bmatrix} 1 \\ 1 \\ \vdots \\ 1 \end{bmatrix} + \begin{bmatrix} 1 & 1 & \dots & 1 \\ c_1 & c_2 & \dots & c_P \\ \vdots & \vdots & \ddots & \vdots \\ c_1^{P-1} & c_2^{P-1} & \dots & c_P^{P-1} \end{bmatrix} \begin{bmatrix} \hat{z}_1 \\ \hat{z}_2 \\ \vdots \\ \hat{z}_P \end{bmatrix} = \begin{bmatrix} 0 \\ 0 \\ \vdots \\ 0 \end{bmatrix}. \quad (\text{A1})$$

The solution³³ to Eq. A1, by using $c_p = q^{-p}$, is

$$\hat{z}_p = -\frac{\prod_{\substack{i=1 \\ i \neq p}}^P (1 - q^{-i})}{\prod_{\substack{i=1 \\ i \neq p}}^P (q^{-p} - q^{-i})}. \quad (\text{A2})$$

In the bottom product of Eq. A2 we factor out q^{-p} , and then split all products into cases when $i < p$ and $i > p$. These modifications are shown in Eq. A3.

$$\begin{aligned} \hat{z}_p &= -\frac{\prod_{\substack{i=1 \\ i \neq p}}^P (1 - q^{-i})}{\prod_{\substack{i=1 \\ i \neq p}}^P q^{-p}(1 - q^{-i+p})} = \\ &= \frac{\prod_{i=1}^{p-1} (1 - q^{-i}) \prod_{i=p+1}^P (1 - q^{-i})}{q^{-p(P-1)} \prod_{i=1}^{p-1} (1 - q^{-i+p}) \prod_{i=p+1}^P (1 - q^{-i+p})} \end{aligned} \quad (\text{A3})$$

Further modification by variable substitution ($i' = i - p$ in the top and bottom right products, and $i' = -i + p$ in the bottom left product) gives Eq. A4.

$$\hat{z}_p = -\frac{\prod_{i=1}^{p-1} (1 - q^{-i}) \prod_{i=1}^{P-p} (1 - q^{-i-p})}{q^{-p(P-1)} \prod_{i=1}^{p-1} (1 - q^i) \prod_{i=1}^{P-p} (1 - q^{-i})} \quad (\text{A4})$$

From Eq. A4 and onward we will re-letter the new index symbol i' with the old i when using variable substitution, *i.e.* $i' \rightarrow i$ in this case. This to avoid multiple indexes and thus confusions with other entities. Further simplification of the two left products (by factoring out q^{-i} from the top one) gives Eq. A5.

$$\hat{z}_p = (-1)^p q^{p(2P-p-1)/2} \frac{\prod_{i=1}^{P-p} (1 - q^{-i-p})}{\prod_{i=1}^{P-p} (1 - q^{-i})} \quad (\text{A5})$$

We now factor out q^{-i-p} from the top product and q^{-i} from the bottom product giving Eq. A6, where we also note the cancellation of the $(-1)^{P-p}$ factors.

$$\hat{z}_p = (-1)^p q^{p(2P-p-1)/2} \frac{\prod_{i=1}^{P-p} q^{-i-p} \prod_{i=1}^{P-p} (1 - q^{i+p})}{\prod_{i=1}^{P-p} q^{-i} \prod_{i=1}^{P-p} (1 - q^i)} \quad (\text{A6})$$

Simplification of the left products yield

$$\hat{z}_p = (-1)^p q^{p(p-1)/2} \frac{\prod_{i=1}^{P-p} (1 - q^{i+p})}{\prod_{i=1}^{P-p} (1 - q^i)}. \quad (\text{A7})$$

By making the variable substitution $i' = P - i - p + 1$ in the top product we get Eq. A8 where we note that the products together are equal to the q -binomial coefficient¹⁴ $\left[\begin{smallmatrix} P \\ P-p \end{smallmatrix} \right]_q = \left[\begin{smallmatrix} P \\ p \end{smallmatrix} \right]_q$.

$$\hat{z}_p = (-1)^p q^{p(p-1)/2} \frac{\prod_{i=1}^{P-p} (1 - q^{P-i+1})}{\prod_{i=1}^{P-p} (1 - q^i)} \quad (\text{A8})$$

Thus we now have arrived at

$$\hat{z}_p = (-1)^p q^{p(p-1)/2} \left[\begin{smallmatrix} P \\ p \end{smallmatrix} \right]_q. \quad (\text{A9})$$

Appendix B: Self-energy

Starting from Eq. 7 we note that if a particle is positioned in the origin, *i.e.* $r = 0$, then the equation becomes

$$\begin{bmatrix} 1 \\ 0 \\ \vdots \\ 0 \end{bmatrix} z + \begin{bmatrix} 1 & 1 & \cdots & 1 \\ r_1 & r_2 & \cdots & r_P \\ \vdots & \vdots & \ddots & \vdots \\ r_1^{P-1} & r_2^{P-1} & \cdots & r_P^{P-1} \end{bmatrix} \begin{bmatrix} z'_1 \\ z'_2 \\ \vdots \\ z'_P \end{bmatrix} = \begin{bmatrix} 0 \\ 0 \\ \vdots \\ 0 \end{bmatrix}. \quad (\text{B1})$$

Here we have indexed the image charges with primes as to distinguish them from the charges when we calculate the potential from a particle at position $r > 0$. Note that in Eq. B1 there is only a charge present due to the centered particle and no higher order moments. Assuming that the image particles needed to cancel this charge (and all higher order moments generated by themselves in the process) are positioned at $r_p = c_p r'$ where $r' > 0$ is any point, then Eq. B1 converts to Eq. B2 which has its solution³³ shown in Eq. B3 where we have used $c_p = q^{-p}$.

$$\begin{bmatrix} 1 \\ 0 \\ \vdots \\ 0 \end{bmatrix} + \begin{bmatrix} 1 & 1 & \cdots & 1 \\ c_1 & c_2 & \cdots & c_P \\ \vdots & \vdots & \ddots & \vdots \\ c_1^{P-1} & c_2^{P-1} & \cdots & c_P^{P-1} \end{bmatrix} \begin{bmatrix} z'_1 \\ z'_2 \\ \vdots \\ z'_P \end{bmatrix} = \begin{bmatrix} 0 \\ 0 \\ \vdots \\ 0 \end{bmatrix} \quad (\text{B2})$$

$$\hat{z}'_p = -\frac{\prod_{\substack{i=1 \\ i \neq p}}^P (-q^{-i})}{\prod_{\substack{i=1 \\ i \neq p}}^P (q^{-p} - q^{-i})} \quad (\text{B3})$$

By condensing these products into one, and splitting the result as to give products for $i < p$ and $i > p$, we get

$$\begin{aligned} \hat{z}'_p &= -\frac{1}{\prod_{\substack{i=1 \\ i \neq p}}^P (1 - q^{-p+i})} = \\ &= -\frac{1}{\prod_{i=1}^{p-1} (1 - q^{-p+i}) \prod_{i=p+1}^P (1 - q^{-p+i})}. \end{aligned} \quad (\text{B4})$$

Variable substitution using $i' = i - p$ in the right product gives

$$\hat{z}'_p = -\frac{1}{\prod_{i=1}^{p-1} (1 - q^{-p+i}) \prod_{i=1}^{P-p} (1 - q^i)} \quad (\text{B5})$$

and by factoring out q^{-p+i} from the left product we get

$$\hat{z}'_p = -(-1)^{p-1} \frac{q^{(p-1)p/2}}{\prod_{i=1}^{p-1} (1 - q^{p-i}) \prod_{i=1}^{P-p} (1 - q^i)}. \quad (\text{B6})$$

Using these moments, the self-energy becomes

$$\frac{E_{\text{Self}}}{\left(\frac{e^2}{4\pi\epsilon_0\epsilon_r} \right)} = \sum_{j=1}^N \frac{z_j^2}{R_c} \sum_{p=1}^P \frac{\left(-(-1)^{p-1} \frac{q^{(p-1)p/2}}{\prod_{i=1}^{p-1} (1 - q^{p-i}) \prod_{i=1}^{P-p} (1 - q^i)} \right)}{q^{-(p-1)}}. \quad (\text{B7})$$

Reshuffling some of the terms in Eq. B7 gives Eq. B8.

$$\begin{aligned} \frac{E_{\text{Self}}}{\left(\frac{e^2}{4\pi\epsilon_0\epsilon_r}\right)} &= \\ &= -\sum_{j=1}^N \frac{z_j^2}{R_c} \sum_{p=1}^P (-1)^{p-1} \frac{q^{(p-1)p/2} q^{(p-1)}}{\prod_{i=1}^{p-1} (1 - q^{p-i}) \prod_{i=1}^{P-p} (1 - q^i)} \end{aligned} \quad (\text{B8})$$

The denominators in Eq. B8 are polynomials with only non-negative powers. Thus if $q \rightarrow 0$ only the constant term 1 will be non-vanishing. In the same limit the nominator will be zero for every $p > 1$ and thus the entire far right sum will equal one in the limit $q \rightarrow 0$, which comes from the term $p = 1$. The final expression (independent of P) for the far right sum in the limit $q \rightarrow 0$ is thus 1 as is shown in Eq. B9. The choice of q seems somewhat arbitrary however our choice of $q \rightarrow 0$ comes from the following arguments: In the original derivation for the potential we chose to mirror the particle position in the cut-off as to get the image particle positions. However this is not possible to do when the particle is in the origin (since then we would have to divide by zero). Thus we choose to mirror an identical particle infinitesimally close ($q \rightarrow 0$) to the origin.

$$E_{\text{Self}} = -\frac{e^2}{4\pi\epsilon_0\epsilon_r R_c} \sum_{j=1}^N z_j^2 \quad (\text{B9})$$

Appendix C: Results for different cut-offs

In Fig. 8 we show the RDF between oxygen atoms using $R_c = 0.96$ nm. The patterns are similar but more enhanced as to the case when using $R_c = 1.28$ nm. The logarithm of the ratio between the pair-potential and Ewald results, Fig. 9, and the angular correlations, Fig. 10, shows this even more clearly. Here we acknowledge that $q(n = 5)$ is most resembling the Ewald results and that $q(n = 7)$ have larger deviations compared to Ewald results than the former. Thus, here $q(n = 5)$ is an optimal choice as compared to Ewald. In Table III we see similar results as to when using $R_c = 1.28$ nm however the trends of the q -potential to overestimate and SP1/SP3 to underestimate the density is reinforced.

In Fig. 11 we show the RDF between oxygen atoms using $R_c = 1.6$ nm. Again, the patterns are similar but now more damped as to the case when using $R_c = 1.28$ nm. The logarithm of the ratio between the pair-potential and Ewald results, Fig. 12, and the angular correlations, Fig. 13, shows this even more clearly. In Table IV we see similar results as to when using $R_c = 1.28$ nm, indicating that a cut-off of 1.28 nm might suffice to produce converged results with respect to the same.

Potential	ρ	ϵ_r	G_K
$q(P = 1)$	1127	2 ± 0	4.8
$q(P = 2)$	1000	75 ± 1	2.7
$q(P = 3)$	997	67 ± 3	2.4
$q(P = 4)$	997	67 ± 4	2.4
$q(P = 5)$	998	76 ± 1	2.7
$q(P = 6)$	999	74 ± 2	2.6
$q(P = 7)$	1000	69 ± 2	2.4
$q(P = 8)$	1001	72 ± 3	2.6
$q(P = \infty)$	1003	72 ± 3	2.5
SP1	988	69 ± 2	2.5
SP3	993	70 ± 2	2.5
Ewald	996	66 ± 2	2.3
Exp.	997	79	-

TABLE III: Values for density ρ in units of kg/m^3 , dielectric constant ϵ_r , and Kirkwood factor G_K for the different potentials using $R_c = 0.96$ nm applied on a bulk water-system and experimental reference³².

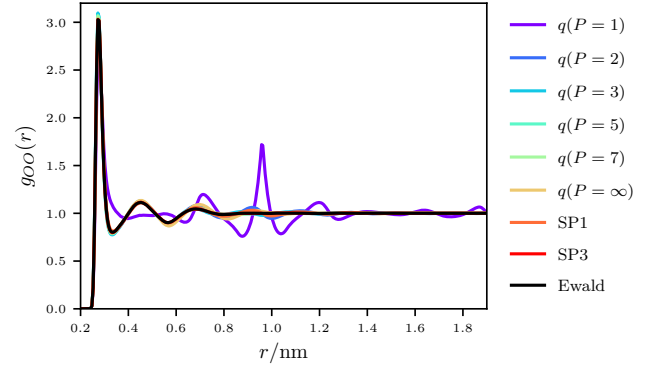


FIG. 8: Oxygen-oxygen pair-correlation function $g_{OO}(r)$ using $R_c = 0.96$ nm. We want the reader to note that most of the curves overlap.

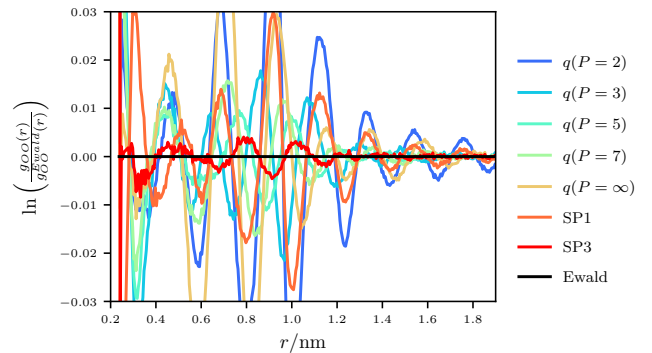


FIG. 9: The logarithm of the ratio between the pair-potential and Ewald results using $R_c = 0.96$ nm.

Appendix D: Kirkwood-Buff Theory

For the simulated \mathcal{NPT} ensemble, we considered the following running integral

$$\hat{G}_{AB}(R) = 4\pi \int_0^R [g_{AB}^{\mathcal{NPT}}(r) - 1] r^2 dr. \quad (\text{D1})$$

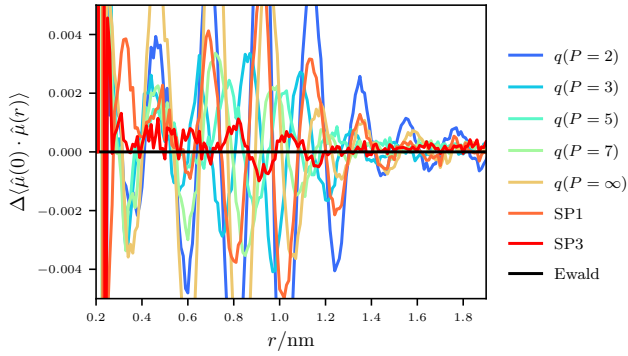


FIG. 10: Difference compared to Ewald results between angular correlations of the normalized dipole-moments $\hat{\mu}$ of the waters using $R_c = 0.96$ nm.

Potential	ρ	ε_r	G_K
$q(P=1)$	1071	2 ± 0	2.8
$q(P=2)$	999	72 ± 1	2.6
$q(P=3)$	999	69 ± 2	2.5
$q(P=4)$	999	70 ± 2	2.5
$q(P=5)$	999	68 ± 1	2.4
$q(P=6)$	999	74 ± 1	2.6
$q(P=7)$	999	70 ± 3	2.5
$q(P=8)$	998	73 ± 3	2.6
$q(P=\infty)$	999	73 ± 1	2.6
SP1	995	71 ± 3	2.5
SP3	997	68 ± 2	2.4
Ewald	996	66 ± 2	2.3
Exp.	997	79	-

TABLE IV: Values for density ρ in units of kg/m^3 , dielectric constant ε_r , and Kirkwood factor G_K for the different potentials using $R_c = 1.6$ nm applied on a bulk water-system and experimental reference³².

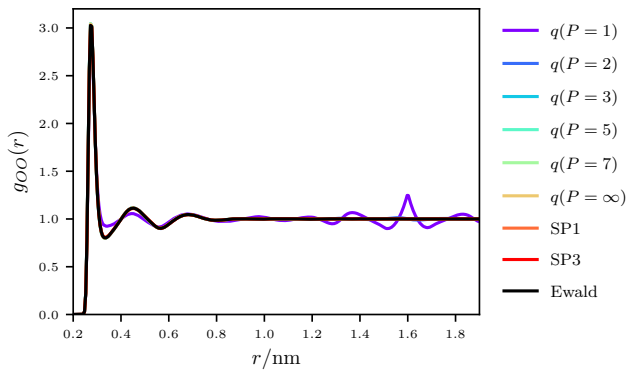


FIG. 11: Oxygen-oxygen pair-correlation function $g_{OO}(r)$ using $R_c = 1.6$ nm. We want the reader to note that all but the $q(n=1)$ -curve overlap.

where the hat indicates that RDFs in the \mathcal{NPT} ensemble is used in place of the ones in the grand canonical ensemble, and R is the distance of truncation. The excess coordination number of component B around component A , *i.e.*, the excess number of particles B around particles A compared to bulk composition, is obtained

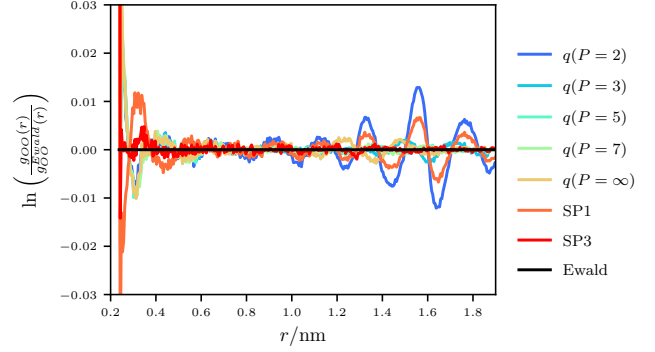


FIG. 12: The logarithm of the ratio between the pair-potential and Ewald results using $R_c = 1.6$ nm.

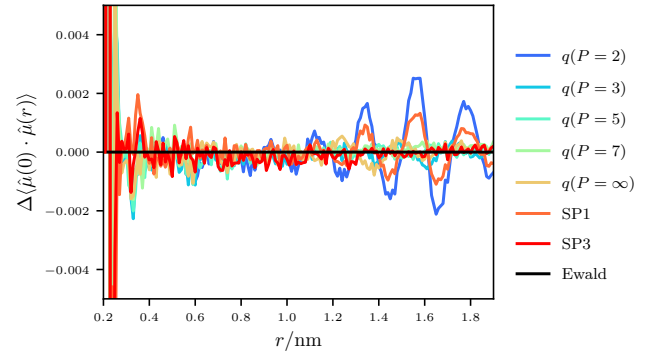


FIG. 13: Difference compared to Ewald results between angular correlations of the normalized dipole-moments $\hat{\mu}$ of the waters using $R_c = 1.6$ nm.

as $\Delta N_{AB} = \rho_B G_{AB}$, where ρ_B is the average number density of particles B in the system.

Due to the finite size of simulated systems, some complications arise when applying KB theory. Firstly, the calculated RDFs usually does not converge within the simulation cell. This is most easily understood considering the excess coordination number $\Delta N_{AB} = \rho_B G_{AB}$. In a finite system containing non-ideal particles, the excess coordination numbers between the particles are non-zero due to interactions. Since the system is finite, an excess or deficit of for instance particles B around particles A will cause a corresponding deficit or excess of particles B in the bulk. Hence the bulk composition, $\rho_{AB}^{(bulk)}$, will be different from ρ_B which is used for normalization according to $g_{AB}(r) = \rho_{AB}(r)/\rho_B$. To make the RDFs asymptotically approach unity, we used the following correction factor^{22,24} which scales the RDF so that it is normalized with $\rho_{AB}^{(bulk)}$ rather than ρ_B

$$C_{AB}^{(1)}(r) = \frac{N_B \left(1 - \frac{V(r)}{V_{cell}}\right)}{N_B \left(1 - \frac{V(r)}{V_{cell}}\right) - \Delta N_{AB}(r) - \delta_{AB}}. \quad (D2)$$

Here N_B is the total number of particles B , $V(r)$ is the volume of a sphere with radius r , V_{cell} is the volume of the simulation cell, and δ_{AB} is the Kronecker delta. In the expression, the nominator is the number of par-

TABLE V: Fitting parameters used to obtain activity coefficients as a function of salt molality using Equation D6.

Salt	b_1	b_2	b_3	b_4
NaCl	1.4369	0.0054	0.0495	0.0092
NaI	1.4681	0.1361	0.0344	-0.0102

ticles B that would occupy the volume beyond r if the composition would be uniform, while the denominator approximates the true number of particles B in the same volume.

$$G_{AB} = \frac{1}{V} \int_V \int_V [g_{AB}^{\mu VT}(r_{12}) - 1] d\mathbf{r}_1 d\mathbf{r}_2 \quad (\text{D3})$$

Secondly, for closed systems one cannot reduce the double integral in Eq. D3 to the single integral in Eq. 15 since the integration domain of r is no longer independent of \mathbf{r}_1 . To account for this, a method has been suggested²⁵ where the exact KBI is found by applying a factor depending on the geometry of the system to the single integral and evaluating the expression in the thermodynamic limit, *i.e.* as $1/R \rightarrow 0$. As an alternative method²⁵, it was suggested that an extrapolated expression of the exact KBI may be obtained by applying the following factor directly in the single integral, which is the method we used,

$$C_{AB}^{(2)}(r) = 1 - \left(\frac{r}{R}\right)^3. \quad (\text{D4})$$

To obtain approximate KBIs accounting for the system being both closed and of finite size, we simultaneously apply the two corrections²³ according to

$$G_{AB} \approx \hat{G}_{AB}^*(R) = 4\pi \int_0^R [g_{AB}^{\mathcal{N}PT}(r) C_{AB}^{(1)}(r) - 1] r^2 C_{AB}^{(2)}(r) dr \quad (\text{D5})$$

where the star indicates that correction factors are applied. For the activity derivatives, the integral was then evaluated at a value of R where convergence is obtained, corresponding to the distance from the center particle at which bulk composition is reached.

The experimental activity coefficients²⁷ were used to find the values of the parameters b_j in the following fitting function³⁴, relating the activity coefficient to the concentration on the molal scale,

$$\ln \gamma(m) = -\frac{1.18\sqrt{m}}{1 + b_1\sqrt{m}} - \ln(1 - b_2m) + b_3m + b_4m^2. \quad (\text{D6})$$

The obtained values of b_j are reported in Table V.

Since the experimental activity coefficients used in this study are on the molal scale, we converted the concentration scale to be in the unit of number density in order to calculate the activity derivatives as $a'_c = (\partial \ln a_c / \partial \ln \rho_c)_{PT}$. For the conversion, we used experimental density data^{35,36}.

TABLE VI: Lennard-Jones parameters for Na^+ , Cl^+ , and I^- . To the right the number of water-molecules in each simulation is presented for the different molalities ($\text{mol}^{-1} \text{kg}^{-1}$).

Salt	Ion	q/e	σ/nm	$\epsilon/\text{kJ}\cdot\text{mol}^{-1}$	\mathcal{N}_{H_2O}		
					1.0	2.0	3.0
NaCl	Na^+	+1.0	0.255	0.280	5963	5252	4672
	Cl^-	-1.0	0.440	0.418			
NaI	Na^+	+1.0	0.255	0.280	5796	5026	4402
	I^-	-1.0	0.491	0.158			

Appendix E: Dielectric constant

The dielectric constant, ϵ_r , has been derived within a known theoretical framework³⁷ where the key equation is

$$\frac{\epsilon_r - 1}{\epsilon_r + 2} \left[1 - \frac{\epsilon_r - 1}{\epsilon_r + 2} \tilde{T}(0) \right]^{-1} = \frac{1}{3\epsilon_0} \frac{\langle M^2 \rangle}{3Vk_B T}. \quad (\text{E1})$$

Here $\langle M^2 \rangle$ are the fluctuations of the dipole moment $\mathbf{M} = \sum_{i=1}^{\mathcal{N}} \boldsymbol{\mu}_i$, k_B is the Boltzmann constant, and V the volume of the unit cell. Different values of $\tilde{T}(0)$ is used pending the method. In the following derivations we want to stress that $q = q(r)$. In order to get first higher order interactions we get

$$\nabla \left(\frac{\mathcal{S}(q)}{r} \right) = \frac{\nabla \mathcal{S}(q)}{r} + \mathcal{S}(q) \nabla \left(\frac{1}{r} \right) \quad (\text{E2})$$

where ∇ is the gradient operator. Further second higher order interactions is then

$$\begin{aligned} \nabla^T \nabla \left(\frac{\mathcal{S}(q)}{r} \right) &= \frac{\nabla^T \nabla \mathcal{S}(q)}{r} + \nabla^T \mathcal{S}(q) \nabla \left(\frac{1}{r} \right) + \\ &+ \nabla^T \left(\frac{1}{r} \right) \nabla \mathcal{S}(q) + \mathcal{S}(q) \nabla^T \nabla \left(\frac{1}{r} \right). \end{aligned} \quad (\text{E3})$$

Note that $\mathcal{S}(q)$ is not angle-dependent and thus

$$\nabla \mathcal{S}(q) = \hat{\mathbf{r}} \frac{\partial}{\partial r} \mathcal{S}(q). \quad (\text{E4})$$

However, by further apply ∇^T to this we get

$$\nabla^T \nabla \mathcal{S}(q) = \hat{\mathbf{r}}^T \hat{\mathbf{r}} \frac{\partial^2}{\partial r^2} \mathcal{S}(q) + \frac{\partial}{\partial r} \mathcal{S}(q) (\mathbf{I} - \hat{\mathbf{r}}^T \hat{\mathbf{r}}). \quad (\text{E5})$$

The total expression for $\nabla^T \nabla (\mathcal{S}(q)/r)$ can be parted like

$$\nabla^T \nabla \left(\frac{\mathcal{S}(q)}{r} \right) = a(r) (3\hat{\mathbf{r}}^T \hat{\mathbf{r}} - \mathbf{I}) + b(r) \mathbf{I} \quad (\text{E6})$$

where

$$a(r) = \frac{\partial^2}{\partial r^2} \mathcal{S}(q) - \frac{\partial}{\partial r} \mathcal{S}(q) \frac{1}{r^2} + \frac{\mathcal{S}(q)}{r^3} \quad (\text{E7})$$

and

$$b(r) = \frac{\partial^2}{\partial r^2} \mathcal{S}(q) \frac{1}{3r}. \quad (\text{E8})$$

In order to get the proper evaluation of the dielectric constant we have to evaluate the integrals³⁷

$$A(k) = -3 \int_0^\infty r^2 j_2(kr) a(r) dr \quad (\text{E9})$$

and

$$B(k) = 3 \int_0^\infty r^2 j_0(kr) b(r) dr. \quad (\text{E10})$$

For $k = 0$, *i.e.* evaluation of the static dielectric constant, the spherical Bessel functions becomes $j_0(0) = 1$ and $j_2(0) = 0$. Therefore $A(0)$ has the trivial solution zero (since the singularity of $a(r)$ in $r = 0$ has been explicitly dealt with³⁷) and we now only have to evaluate $B(0)$. Thus we have

$$B(0) = \int_0^{R_c} r \frac{\partial^2}{\partial r^2} \mathcal{S}(q) dr \quad (\text{E11})$$

where the limit ∞ has changed to R_c due to the fact that we use $\mathcal{S}(q) \equiv 0$ for $q > 1$, that is $r > R_c$. Integration by parts gives

$$B(0) = \left[r \frac{\partial}{\partial r} \mathcal{S}(q) \right]_0^{R_c} - \int_0^{R_c} \frac{\partial}{\partial r} \mathcal{S}(q) dr = 1 \quad (\text{E12})$$

which is true for all the tested pair-potentials except q -potential using $P = 1$ where $B(0) = 0$. Finally we note that $\tilde{T}(0) = B(0)$ and thus the derivation is done. Note that the derived formula using the $q(P = 1)$ -potential is known to represent high dielectric medium poorly³¹ and should thus be used carefully.

¹R. Bell, Transactions of the Faraday Society **27**, 797 (1931).

²P. P. Ewald, Annalen der Physik **369**, 253 (1921).

³H. Kornfeld, Zeitschrift für Physik A Hadrons and Nuclei **22**, 27 (1924).

⁴J. Kolafa and J. W. Perram, Molecular Simulation **9**, 351 (1992).

⁵Z. Wang and C. Holm, The Journal of Chemical Physics **115**, 6351 (2001).

⁶T. Darden, D. York, and L. Pedersen, The Journal of Chemical Physics **98**, 10089 (1993).

⁷D. Wolf, P. Keblinski, S. Phillpot, and J. Eggebrecht, The Journal of chemical physics **110**, 8254 (1999).

⁸P. Demontis, S. Spanu, and G. B. Suffritti, The Journal of Chemical Physics **114**, 7980 (2001).

⁹D. Zahn, B. Schilling, and S. M. Kast, The Journal of Physical Chemistry B **106**, 10725 (2002).

¹⁰C. J. Fennell and J. D. Gezelter, The Journal of Chemical Physics **124**, 234104 (2006).

¹¹G. S. Fanourgakis, T. E. Markland, and D. E. Manolopoulos, The Journal of chemical physics **131**, 094102 (2009).

¹²Y. Yonezawa, The Journal of Chemical Physics **136**, 244103 (2012).

¹³I. Fukuda, The Journal of chemical physics **139**, 174107 (2013).

¹⁴L. Comtet, *Advanced combinatorics: the art of finite and infinite expansions. 1974* (Reidel, Dordrecht).

¹⁵V. G. Kac and P. Cheung, *Quantum calculus* (Springer, 2002).

¹⁶B. Stenqvist and M. Lund, EPL (Europhysics Letters) **123**, 10003 (2018).

¹⁷P. Eastman, M. S. Friedrichs, J. D. Chodera, R. J. Radmer, C. M. Bruns, J. P. Ku, K. A. Beauchamp, T. J. Lane, L.-P. Wang, D. Shukla, T. Tye, M. Houston, T. Stich, C. Klein, M. R. Shirts, and V. S. Pande, J. Chem. Theory Comput. **9**, 461 (2013).

¹⁸J. Åqvist, P. Wennerström, M. Nervall, S. Bjelic, and B. O. Brandsdal, Chem. Phys. Lett. **384**, 288 (2004).

¹⁹D. A. Sivak, J. D. Chodera, and G. E. Crooks, J. Phys. Chem. B **118**, 6466 (2014).

²⁰J. G. Kirkwood and F. P. Buff, The Journal of Chemical Physics **19**, 774 (1951).

²¹S. Weerasinghe and P. E. Smith, The Journal of Chemical Physics **119**, 11342 (2003).

²²B. Hess and N. F. A. van der Vegt, Proc. Natl. Acad. Sci. U. S. A. **106**, 13296 (2009).

²³J. Milzetti, D. Nayar, and N. F. A. van der Vegt, J. Phys. Chem. B, [Online early access] (2018).

²⁴P. Ganguly and N. F. A. van der Vegt, J. Chem. Theory Comput. **9**, 1347 (2013).

²⁵P. Krüger, S. K. Schnell, D. Bedeaux, S. Kjelstrup, T. J. H. Vlugt, and J.-M. Simon, J. Phys. Chem. Lett. **4**, 235 (2013).

²⁶A. Ben-Naim, *Statistical Thermodynamics for Chemists and Biochemists* (Plenum: New York, 1992).

²⁷R. A. Robinson and R. H. Stokes, *Electrolyte Solutions*, 2nd ed. (Butterworths: London, 1959) pp. 492–494.

²⁸G. Tesei, V. Aspelin, and M. Lund, The Journal of Physical Chemistry B **122**, 5094 (2018).

²⁹L. X. Dang, Journal of the American Chemical Society **117**, 6954 (1995).

³⁰P. H. Hünenberger and J. A. McCammon, Biophysical chemistry **78**, 69 (1999).

³¹D. Adams and I. McDonald, Molecular Physics **32**, 931 (1976).

³²H. S. Harned and B. B. Owen, “The physical chemistry of electrolytic solutions,” Tech. Rep. (Reinhold Pub. Corp., 1958) page 161.

³³M. E. El-Mikkawy, Applied Mathematics and Computation **146**, 643 (2003).

³⁴M. B. Gee, N. R. Cox, Y. Jiao, N. Benteitis, S. Weerasinghe, and P. E. Smith, J. Chem. Theory Comput. **7**, 1369 (2011).

³⁵I. D. Zaytsev and G. G. Aseyev, *Properties of Aqueous Solutions of Electrolytes* (CRC Press, 1992) pp. 1724–1727.

³⁶M. Laliberté and W. E. Cooper, J. Chem. Eng. Data **49**, 1141 (2004).

³⁷M. Neumann, Molecular Physics **57**, 97 (1986).